Summer temperature fluctuations in Southwestern China during the end of the LGM and the last deglaciation

Enlou Zhang[1*], Jie Chang[1,2], James Shulmeister[2], Pete Langdon[3], Weiwei Sun[1], Yanmin Cao[4], Xiangdong Yang[1] and Ji Shen[1]

1. State Key Laboratory of Lake Science and Environment, Nanjing Institute of Geography and Limnology, Chinese Academy of Science, Nanjing 210008, China
2. School of Earth and Environmental Sciences, The University of Queensland, St Lucia, Qld 4072, Australia
3. Geography and Environment, University of Southampton, Southampton SO17 1BJ, UK
4. College of Resources and Environmental Science, South-Central University for Nationalities, Wuhan 430074, China

*__Corresponding author:__ elzhang@niglas.ac.cn

Key words: Chironomidae; paleo-temperature; Indian Summer Monsoon; high latitudes; Southern Ocean; land-ocean-atmosphere interaction

Abstract

We present a sub-centennial resolution summer temperature record from the SE Tibetan Plateau (Tiancai Lake, SW China, 3900 m a.s.l.) derived from a chironomid stratigraphy covering the last c.19.5 ka. The record highlights the interaction between tropical and high-latitude climate forcing through the changes in atmospheric circulation during the last deglaciation. The scale of the last glacial maximum (LGM) cooling is consistent with other tropical mountain regions at c.5 °C and a rapid recovery of temperatures at 19.0 ka is related to changes in adiabatic lapse rates at the end of the glaciation. The overall pattern of change shows that North Atlantic deglaciation climate events (the Heinrich 1 and Younger Dryas cooling events and the Bølling-Allerød warm period) are all recorded, but the influence of the events decline as the deglaciation progresses. We relate these patterns to North Atlantic Deep water ventilating the Southern Ocean and to the consequent movements of the Intertropical Convergence Zone (ITCZ) in the Indian Ocean Basin as transmitted through changes in the southern mid-latitude circulation.

1. Introduction

Environmental changes that occur during deglacial phases are complex and multiple lines of evidence are required to understand key processes beyond simply the rate, timing and magnitude of change. Understanding how the oceans, atmosphere and land interact in terms of heat transfer has become important to understanding the relative strength of monsoon processes, which dominate the climate of the (sub)tropics. Proxy records covering the last deglaciation (c.19-11.7 ka) suggest a bi-polar see-saw mechanism, where heat transfer between the two polar hemispheres works in anti-phase (as reviewed by Shakun and Carlson (2010)). During the early part of the deglaciation (c.19-15 ka), a rise in global temperatures led to rapid ice sheet melting, and increased input of freshwater ot the ocean led to a slowdown or shut down of Atlantic Meridional Ocean Circulation (AMOC) (McManus et al. 2004). This reduction in AMOC would have caused a southward shift in the Intertropical Convergence Zone (ITCZ), which in turn changed latitudinal precipitation and wind patterns, as well as upwelling regimes (Lea et al. 2003; Yancheva et al. 2007; Zhang and Delworth 2005). $\delta^{18}O$ records of Chinese cave speleothems show a weakened monsoon during this period (e.g. Wang et al. 2001; Dykoski et al. 2015). These changes, during a weakened AMOC, would result in reduced northward heat transport and it has been suggested that heat may be preferentially stored in the subtropics and tropics (Carlson et al. 2008; Rühlemann et al. 1999), causing at least regional warming in the tropics during North Atlantic cooling events.

These ideas are little tested in terrestrial areas of the tropics, and subtropics and terrestrial temperature reconstructions in these areas rarely extend back to the LGM. Here we develop

the first terrestrial summer temperature record from lake sediments in the Yunnan region of the Qinghai-Tibetan Plateau (QTP) that extends back to the end of the last glacial maximum (LGM). in order to examine climate responses in this region during the deglaciation, while the Asian summer monsoon was inferred to be weakened (Shakun et al. 2007; Wang et al. 2001). In addition, we compare our summer temperature reconstruction with a model simulation of regional mean annual temperatures based on the output data from the TraCE-21000 model experiment which is forced by meltwater flux, orbital changes, CO_2, and ice sheet volume (Liu et al. 2009). We aim to understand the rate, magnitude and timing of changes in terrestrial summer temperatures to better understand the long-term nexus of the regional summer temperature and the Asian summer monsoons.

The Yunnan region of the QTP forms an important eastern extension of the Tibetan high country (Fig. 1). It differs from the main QTP in that it is primarily influenced by warm and humid airflow from the Bay of Bengal in summer and is much more humid than the high plateau areas. The Yunnan high altitude region extends to over 4200 m a.s.l. and glaciers occupied valleys down to at least 3700 m a.s.l. during the last glaciation (Zhang et al. 2015). Lakes formed in the cirque basins after the glaciers retreated. We have no direct age evidence for the latest ice occupation of the lake basin but basal sediment ages indicate that the study basin was ice-free by 19.5 ka. Consequently, this lake (Tiancai Lake) records changes from the termination of the LGM to modern times, including the whole of the last deglaciation (c.19-11.7 ka). On and around the QTP, there are a variety of records that indicate changes in precipitation (Wang et al. 2014; Opitz et al. 2015), but there are very few proxies for temperature change, except pollen-based reconstructions from more arid areas of the QTP (Opitz et al. 2015; Shen et al. 2006) and none for seasonal temperatures. Here we present

summer temperatures reconstructed from chironomids, at sub-centennial scale from 19.5 ka from Tiancai Lake, an alpine lake located in northern Yunnan Province (Fig. 1).

2. Materials and Methods

2.1. Study site

Tiancai Lake (26°38′3.8″N, 99°43′00″E, 3890 m a.s.l.) has a surface area of c.2.1 ha, a mean depth of 6 m and is located in the SE edge of the Tibetan Plateau, Yunnan Province, SW China (Fig. 1). The lake is in the lower part of a chain of glacially-carved lakes. It is hydrologically open with three inflows from the west, south and southeast, and has an outflow to the north. The climate in this region is strongly influenced by the Indian Ocean (Andaman Sea) Monsoon (Fig. 1), with a mean annual temperature at Tiancai Lake of c.2.5 °C, mean July temperature of 8.4 °C and mean annual precipitation of c.910 mm falling mainly between July and September. The lake freezes in winter. Primary forest above 3200 m is characterized by montane conifers such as *Abies georgii, Picea* sp. and evergreen broadleafs notably *Rhododendron* spp. (Xiao et al. 2014). The upper catchment above 4000 m a.s.l. is dominated by Ericaceae, while the summit area around 4200 m a.s.l is an alpine meadow (Xiao et al. 2014). The lake sediment is organic rich, with a pH value of 7.45 and conductivity of 11 μS cm^{-1} (in October 2006) (Chen et al. 2014b). The lake basin became deglaciated after c.19.5 ka and the lake was rapidly established (Zhang et al. 2005). Tiancai Lake is an ideal place for investigating the activity of the Asian monsoon system, as it is situated in the ecologically and climatically sensitive timberline area, is a headwater basin, and features a continuous and high-resolution stratigraphic record (Xiao et al. 2014; Chen et al. 2014b).

2.2. The sediment core collection and chronology

A 926 cm long core (TCK1) was extracted from the centre of the lake at a water depth of 6.8 m using an Uwitech Coring Platform System in 2008, and sectioned at 1-cm intervals. This core did not reach the base of the sediments. In November 2010, another core was collected that reached the rock floor of the basin near core TCK1 using the same piston corer. The second core (TCYL1) is 865-cm-long, and was also sectioned at 1 cm intervals. The two cores, TCK1 and TCYL1 were correlated using radiocarbon chronologies and magnetic susceptibility. A composite core record was constructed for Tiancai Lake with a total length of 1084 cm. The 926 cm sediment of TCK1 and the 707-824 cm (the organic section) of TCYL1 were treated for chironomid analyses, with a total length of 1043 cm of organic sediment. This study mainly discussed the bottom 386 cm (covers c.19.5-8 ka) of the composite sediment record whereas the details of the top sections covering the entire Holocene were included in Zhang et al. (2017b). The chronology was established using ^{210}Pb, 18 accelerator mass spectrometry (AMS) radiocarbon dates on the TCK1 core and 12 AMS dates in the lower part of the TCYL1 core. Detailed chronology results are presented along with the pollen records (Xiao et al., 2014a and Xiao et al., 2014b).

2.3. Chironomid sample preparation and identification

Sub-fossil assemblages of chironomid head capsules preserved in lake sediments have been extensively used to reconstruct variations in summer air temperature across the globe (e.g. Brooks and Langdon, 2014; Chang et al. 2015;). Samples for chironomid analysis were prepared at 4-cm intervals. Chironomid samples were placed in a solution of 10% KOH and

heated to around 75 ºC for 15 minutes. The samples were then sieved with a 90µm mesh and the residue was examined under a stereo-zoom microscope at 25×. All the head capsules found were picked and mounted on microscope slides in a solution of Hydromatrix®. The chironomid head capsules were identified following the chironomid identification guides developed for the Northern Hemisphere and China (Oliver and Roussel 1982; Rieradevall and Brooks 2001; Tang 2006; Brooks et al 2007;). It is somewhat difficult to distinguish specimens of the *Cricotopus*, *Orthocladius* and *Parakiefferiella* genera because of the poor integrity of head capsules, so these fossils were classified as a COP complex in the record (Fig. 2).

2.4. Quantifying summer temperatures and reconstruction validation

The summer air temperatures based on chironomid assemblages of Tiancai Lake were calculated using a chironomid-mean July temperature transfer function (Zhang et al. 2017a) in C2 software (Juggins 2005). This transfer function was built using a WA-PLS model based on 100 lakes that covers all of SW China (Zhang et al. 2017a). It has an r^2 of 0.63 and a sample specific error of ± 2.3°C. Though the error of the transfer function is relatively high compared to the average of c.1 °C from Europe and North America (Brooks and Birks 2001), the trends within the data are likely to be robust as it tracks clearly changes in species assemblages along with the summer temperature gradient (Fig 3).

We applied reconstruction diagnostics including the goodness-of-fit analysis, passive ordination and modern analogue techniques to examine the reliability of the reconstructions using R program (R Core Team 2013) with the package ‘analogue’ developed by Simpson and Oksanen (2016): Goodness-of-fit to mean July temperature was evaluated by passively

fitting fossil samples to the canonical correlation analysis (CCA) ordination axis, which was calculated based on the modern training set of chironomid samples constrained to mean July temperature. Fossil samples whose squared residual length was larger than the residual distance of the extreme 5% of the training set are considered to have a 'poor' fit to temperature. Fossil chironomid samples from 19.5-8 ka were plotted passively and connected with time-tracks on the redundancy analysis plot of the modern training set samples and an overlay of the mean July temperature gradient was also plotted on the same diagram (Fig 3). The modern analogue technique was applied to obtain estimates of the dissimilarity coefficient to the closest modern analogue for each fossil sample. Samples were considered as having 'Good', 'Fair' and 'None' analogue if they have a chi-square distance to the closest modern sample that are larger than the 5^{th} , 15^{th} percentile or beyond of all chi-square distances in the modern assemblage data, respectively (Anderson 1984).

3. Results

3.1. The sediment age vs. zones of the chironomid stratigraphy

We adapted the radiocarbon age model constructed in Xiao et al. (2014a) and Xiao et al. (2014b) as the subsamples were collected from the same core. According to the age-depth model, the composite depths of 1043 - 656 cm are presumed to date to between 19.5 to 8 ka BP. A total of 136 chironomid samples, ranging from 42 to 385 head capsules per sample, were sorted from the sediment samples of this section of the record. All chironomids were identified into 40 genera and 54 species. Of these, 48 taxa had a minimum abundance Hill's N >2% and occurred in more than one sample. Cluster analysis (Grimm 1987) divided the sediment chironomid record into five main zones (Fig. 2). Figure 2 is a summary diagram of

30 major taxa which had an abundance of over 10% and occurred in over 10 samples (N and N2 > 10). The full diagram showing all 48 non-rare chironomid taxa is available as supplementary Figure S1.

Zone 1 from 19.5 to 18.6 ka (1043-1024 cm), *Pseudodiamesa* was the most abundant chironomid taxon in this zone with a mean percentage of 70.8%, decreasing upwards through this zone. Combined with COP complex and *Diamesa* taxa, they comprised 80% of all chironomids with the latter two taxa peaking at 1020 cm (18.3 ka) and 1025 cm (18.7 ka), respectively. *Micropsectra radialis*-type gradually increased across this zone and the abundance reached 29% from an initial value of 1%. Other taxa, except for *Pagastia*, occurred sporadically and showed very low percentages in this stage.

Zone 2 from 18.6 to 14.8 ka (1024-969 cm), was dominated by *Micropsectra radialis*-type (average 26%) and *Heterotrissocladius marcidus*-type (average 14%). The former species reached its two peaks at around 980 cm (15.4 ka) and 920 cm (12.1 ka), while *Heterotrissocladius marcidus*-type began to increase at the end of zone 1 and maintained a relatively high percentage in zone 2. Compared with Zone 1, *Diamesa* displayed very low abundance besides a momentary peak around 995 cm (c.16.1 ka). The COP complex decreased and *Pseudodiamesa* declined significantly after a small peak at 995 cm (c.16.1 ka). Several new taxa emerged in this stage, including *Macropelopia*, *Paramerina*, *Protanypus*, *Eukiefferiella claripennis*-type, *Corynocera ambigula*-type, *Micropsectra* type A, *Micropsectra* type B and *Neozavrelia*, although most of them displayed relatively low abundance.

Zone 3 from 14.8 to 13.1 ka (969-953 cm), *Heterotrissocladius marcidus*-type and *Micropsectra radialis*-type continued dominating the species assemblages however compared to zone 2, *Heterotrissocladius marcidus*-type showed a clear increase in the abundance (from an average 14% to 20.4%) and *Micropsectra radialis*-type declined (from average 26% to 21.5%). *Heterotrissocladius marcidus*-type remained high through this zone and reached its peak (27%) at around 967 cm (14.6 ka) while *Micropsectra radialis*-type reached its minimum (14%) at around 959 cm (13.6 ka). Compared with Zone 2, taxa such as *Pseudodiamesa*, COP complex, *Micropsectra insignilobus*-type, *Corynocera ambigula*-type all showed an apparent decline. In contrast, *Tvetenia tamafalva*-type, *Parametrina*, *Micropsectra* type B showed increases in their abundance.

Zone 4 from 13.1 to 11.6 ka (953-888 cm), is characterized by the predominance of *Micropsectra radialis*-type with an average of 29.7% and a rising trend that started at the end of zone 3 and reached its peak (47.8%) at 924 cm (12.2 ka). *Heterotrissocladius marcidus*-type continued to co-dominate the assemblages until half-way through this zone, where it declined (from an average of 16.5% to 9.1%) at around 924 cm (12.2 ka). Compared with zone 3, most of the other taxa displayed very minor fluctuations but, *Eukiefferiella claripennis*-type, *Tvetenia tamafalva*-type and *Micropsectra insignilobus*-type all increase in abundance from about 920 cm (c.12.1 ka).

Zone 5 from 11.6 to 8 ka (888-656 cm), several new taxa were more abundant than before, and the chironomid diversity increased. Except for *Heterotrissocladius marcidus*-type, other dominant taxa (e.g. *Tvetenia tamafalva*-type, *Micropsectra radialis*-type and *Micropsectra insignilobus*-type) displayed small apparently random fluctuations through this zone. *Heterotrissocladius marcidus*-type, *Micropsectra radialis*-type and *Pseudodiamesa*

249 decreased from c.895 cm, (c.11.6 ka), whereas *Tvetenia tamafalva*-type, *Micropsectra*
250 *insignilobus*-type and *Eukiefferiella claripennis*-type maintained similar percentages from the
251 end of zone 4 and remained at relatively high abundance. *Chironomus* and *Procladius* genera
252 began to occur although with low abundance.
253
254 3.2. The reliability of the summer temperature reconstructions
255
256 The goodness-of-fit results show that only seven fossil samples (about 5% of the total
257 samples) whose squared residual length were larger than the residual distance of the extreme
258 5% of the training set, and were considered to have a relatively 'poor' fit to temperature (Fig.
259 3A). The trajectory changes of the fossil samples generally track the mean July temperature
260 gradient suggesting the influence of the secondary gradient on these fossil samples is
261 insignificant (Fig. 3B). The modern analogue technique analyses show that a total of 17
262 samples (about 12.5 % of total samples)- that is most fossil sample from between 19.5-18.5
263 ka- have 'no analogues' in terms of assemblages within the calibration dataset; seven fossil
264 samples have 'fair analogues'; and 112 fossil samples (about 82 % of total samples) have
265 'good analogues' (Fig. 3C). The overall diagnostics suggest that the mean July temperature
266 reconstructions, particularly during the deglacial and early Holocene (from 18.5-8 ka) are
267 reliable although nearly all samples from 19.5-18.5 ka have no analogues. We acknowledge
268 that the inferred absolute values of the mean July temperatures of the first 1 ka of the record
269 should be interpreted with caution, however, we argue that we should not disregard these
270 results because in many cases, fossil samples with no modern analogues still provide reliable
271 and robust trends in temperature reconstructions (Lotter et al. 1999) as the (WA) PLS model
272 performs relatively well in no analogue situations (Birks 1995; Lotter et al. 1999).
273

More importantly, while the chironomid assemblages have no modern analogues, the LGM component of the record is dominated by a chironomid taxon that is a known cold stenotherm (*Pseudodiamesa*), so it is perfectly reasonable for the model to reconstruct cooler temperatures at this time. *Pseudodiamesa* and *Diamesa spp.* are flowing water associated taxa that indicate that the 'no analogue' result, based on assemblages, not individual taxa, is because the lake is gradually filling at this time, with these taxa likely washed in from the inflow stream.

3.3. Summer temperature variations during the end of the LGM and the last deglaciation

We demonstrated that the reconstructed summer temperature trends track clearly the changes in chironomid taxon assemblages (Fig. 2 and Fig. 4A). The chironomid-derived temperature record reveals that mean July air temperature around Tiancai Lake was c. 3 °C prior to 19.5 ka when the basin was first deglaciated (Fig. 4A), yielding a cooling of 5.4 °C compared to today. There was an initial warming during the period between 18.6 and 11.7 ka, which is offset by a cooling during Heinrich Stadial 1 (HS1, c.17-15 ka), centred on 16.8 ka, but then recovered between 16.4-16.1 ka. This pattern is very similar to that from SSTs in the Arabian Gulf sector of the Indian Ocean (Tierney et al., 2016) and suggests that our record is mirroring changes in the Indian Ocean. It is also consistent with the work from the Andaman Sea by Rashid et al. (2007) who highlight H1 and YD events. The record then shows a relative decline in summer air temperatures until 14.8 ka. Thereafter,weak warming occurred from 14.8 to 12.8 ka which coincides with the Bølling-Allerød (B/A) stage, and a minor cold reversal from 13.1 to 11.6 ka which approximates the Younger Dryas chron (Fig. 4A) and is again observed in both Rashid et al. (2007) and Tierney et al. (2016). From 11.6 ka to 8 ka,

the mean summer temperatures shows minor cooling relative to the present (0.5 °C) (Fig. 4A), and the Holocene sequence is discussed in Zhang et al (2017a) while here we focus on the deglacial phase.

4. Discussion

4.1. Summer cooling at the end of the LGM and the possible mechanisms

The reconstructed LGM summer temperature (c. 3 °C, c. 5.4 °C of cooling from present day) is cooler than expected compared to regional pollen records. A record from Lake Xingyun (1700 m a.s.l) in SW China suggests that the temperature dropped 3 °C during 28-17.6 ka (Chen et al. 2014), whereas a pollen record from Lake Yidun (4400 m a.s.l) on the SE QTP estimated that summer air temperature at c.17.0 ka was 4 °C colder than modern (Shen et al. 2006). Estimates of LGM SSTs of the low latitude oceans are widely variable, both in the scale of the change and in regional expression. For the warmest parts of the tropical ocean (the West Pacific Warm Pool), estimates of LGM cooling range from 1°C to about 4°C. SSTs from foram assemblages and alkenones typically give cooling of ~1°C (e.g. Liu et al., 2002; MARGO, 2009). Most climate models predict about 2°C of cooling (Huang et al., 2013; and see Fig 2A in Tripati et al., 2014) while salinity corrected Mg/Ca estimates (Mathien-Blard and Bassinot, 2009) clumped isotopes (Tripati et al., 2014) support up to 4°C of cooling. These discrepancies have not been satisfactorily resolved but the weight of data and model results suggest that 1-2°C cooling is most likely.

The monsoon region that we are focussing on is the Andaman Sea/Bay of Bengal sector of the Indian Ocean which is the source area for the monsoon in the Yunnan. Again, the records

diverge. Mg/Ca SST estimates (Rashid et al., 2007) for the latter part of the LGM (c. 23-19 ka) indicate about 3°C of cooling whereas foram assemblages (CLIMAP, 2001) and alkenones from the Bay of Bengal (Kudrass et al., 2001) suggest 1-2°C. In either case, these values are substantially less than the c. 5°C we infer from our site during the latest LGM. In contrast, our estimates are compatible with synthesized records based on terrestrial proxies from tropical high altitude mountains which suggest mean annual cooling of 4-6 °C during the LGM (Barrows et al. 2011; Pinot et al. 1999). In addition, reconstructed mean annual air temperature from the Chinese Loess Plateau, c.10° latitudes north of Tiancai Lake, all suggest a 6-7 °C cooling during the LGM (Eagle et al. 2013). This agrees with previous models that suggest greater cooling at high altitude and higher latitude regions as compared to the tropical oceans (Fig. 4D) (Clark et al. 2012; Liu et al. 2009; Shakun et al. 2012).

Glacial climates are generally interpreted to be drier than modern, and there is evidence to suggest that cooling during the LGM was amplified with elevation, leading to significantly steeper lapse rates (Blard et al. 2007; Loomis et al. 2017). Moist adiabatic lapse rates approximate 6 $K.km^{-1}$. Modern values for summer lapse rates in Yunnan are likely to be close to this value as the air is both humid and tropical at lower elevations. The lapse rate for a perfectly dry atmosphere is 9.8 $K.km^{-1}$. A shift in the lapse rate of the order of 1 $K.km^{-1}$ per kilometre to a lapse rate of ~7 $K.km^{-1}$ would account for the observed difference in summer cooling between sea-level in the adjacent Indian Ocean and Tiancai Lake. This level of lapse rate modification is quite modest and average values of about 7 $K.km^{-1}$ are observed in modern meteorological data sets. Therefore, our data are consistent with a reduction in saturation water vapour in the late LGM atmosphere on the order of 15-20%. This provides a mechanism for reconciling summer temperatures from Tiancai Lake with the adjacent tropical oceans that are the regional monsoon source.

An alternative (and/or additional) model is that advection of relatively dry air masses into the inter-tropical convective cells may have played a role (Tripati et al., 2014). This allows under-saturated air to be convected to high elevations and thereby allows much more rapid cooling of the air mass. Tripati et al. (2014) suggest that this mechanism is sufficient to explain the difference between observed and expected tropical glacial snowlines in the West-Pacific Warm Pool when an oceanic cooling of about 4°C is inferred (in this case from clumped isotopes) but it cannot resolve the difference on its own, if oceanic cooling was only 1-2°C. This mechanism can assist in narrowing the change between snowlines and SSTs in the tropics allowing for lesser overall cooling.

The rapid temperature recovery to near modern values at Tiancai Lake between 19.2-18.5 ka indicates a climatic transition from a glacial lapse rate to an interglacial (modern) one. This is supported by the pollen record from this site where forest rapidly reoccupied the basin by around 18.5 ka (Xiao et al. 2014) indicating rapid warming.

Alternatively, the large cooling obtained at the end of the LGM of the record could be due to the enhanced cold water input into local lake waters, through long lasting snow patches or residual glacial ice in the catchment. This has the effect of reducing the water temperature to below its natural relationship with air temperature, allowing preferentially cool water chironomids to inhabit the lake, and thus producing cooler temperatures than would be expected. This has been argued for some Norwegian lakes where cooler than expected air temperatures are reconstructed from recent sediments, as compared with modern instrumental measurements, and this only occurs in lakes that have residual snow patches that last into summer (Brooks and Birks, 2001). However, we argue that this effect is unlikely to have had

a significant impact on the summer temperature reconstructions at Tiancai Lake. This is because frst, the transfer function used was a WAPLS mode, which normally underestimates temperatures at warm sites and overestimates them from colder sites. Tiancai Lake is one of the coldest among the 100-lake training set (Zhang et al., 2017b), thus, the summer temperature of 3°C at the site during the LGM is unlikely an underestimation. Second, we note that a few cold, lotic taxa, such as *Diamesa* were down-weighted in the model-based temperature estimates, as they are rarely present in the modern training set.

4.2. The regional patterns of summer temperature variations during the last deglaciation

There are a few other studies in SW China that detect the North Atlantic-derived, H1, BA and YD events. Specifically, these other records are based on pollen from Tiancai Lake and Lake Naleng, SE QTP and a membrane lipids record from Nam Co, southern QTP (Kramer et al. 2010; Xiao et al. 2014; Günther et al. 2015), but none of these proxies yield an explicitly summer record. Most importantly, these millennial-scale events are present in SST records from the tropical Indian Ocean (Rashid et al., 2007; Tierney et al., 2016). They are also visible in terrestrial records from the wider south and east Asia region including $\delta^{18}O$ records from Hulu Cave and Dongge Cave in SE China and Mawmluh Cave in northern India (Fig. 4J) (Wang et al. 2001; Dykoski et al. 2005; Dutt et al. 2015). These cave sites display a weak or absent monsoon pre-14.8 ka, whereas our record, like the Indian Ocean SST records show warm intervals between 19.5-14.8 ka, indicating an active monsoon but with considerable variability. Our record (Fig. 4A) suggests that the amplitude of cooling events during the deglaciation rapidly declined with a strong 18.5 ka event of about 500 years duration coincident with AMOC shutdown (McManus et al. 2004), a weakened but still clear response

to the H1 event, and a cooling response from c. 15.2-14.8 ka which may be a response to AMOC overshoot (Liu et al. 2009) and may be observed in the modelled temperature response (Fig. 4E). Conversely, the cooling response at the YD is modest compared with the Hulu and Dongge cave records (Fig. 4J). With the exception of the possible AMOC overshoot event, these excursions align rather well with the SST records from both Rashid et al., (2007) in the Andaman Sea and Tierney et al. (2016) (Fig. 4H) in the Arabian Sea sector of the Indian Ocean, supporting the concept that they are directly linked to monsoon strength. Tierney et al. (2016) make an explicit link between their SSTs and changes in the North Atlantic overturn circulation.

The less marked YD signature, and slower but steady warming thereafter contrasts with the rapid changes seen in the Greenland ice core and North Atlantic records (Fig. 4C and 4G), and follows more closely increases in Northern Hemisphere insolation (Fig. 4I) and CO_2 (Fig. 4K) (Berger and Loutre, 1991; Ahn et al., 2004), similar to the modelled temperature response (Fig. 4E) and other tropical records (e.g. Partin et al. 2015) (Fig. 4H). This suggests that there is a progressive increase in tropical influences at our site as the deglaciation period progressed.

4.3. Potential forcing mechanisms of deglacial summer temperature variability

The overall pattern of summer air temperatures during the deglaciation at Tiancai Lake appears to be disconnected from orbitally-induced summer insolation change at 30 °N (Fig. 4I) and the associated increase in atmospheric CO_2 concentrations based on Antarctic records (Fig. 4K) over these deglacial time periods (Ahn et al. 2004). Conversely, they appear more similar to the variations of SSTs from the Indian and the extra-tropical Atlantic oceans (Fig.

4G and 4H) (Rashid et al., 2007; Carlson et al., 2008). The millennial temperature fluctuations are consistent with the timing of North Atlantic climate anomalies (Fig. 4F), implying that shifts in atmospheric or oceanic circulation may have played an important role in climate change around the SE QTP (Fig. 4C, 4F and 4G). During the last deglaciation, North Atlantic climate anomalies have been explained by the variability in strength of AMOC, resulting in modified heat transport to the high latitudes in the northern hemisphere (Bond et al. 1997). The North Atlantic $^{231}Pa/^{230}Th$ record (Fig. 4F) (McManus et al. 2004) shows that a slowdown or complete shutdown of AMOC between c.18-14.8 ka was due to the large volumes of freshwater discharged into the North Atlantic resulting from the melting of both the Laurentide and Fennoscandian ice sheets (McManus et al. 2004). Low North Atlantic SSTs (Fig. 4G), during this cold period led to an increase in the meridional temperature gradient and southward migration of the Intertropical Convergence Zone (ITCZ) (Porter and An 1995), and is inferred to have resulted in a generally weakened East Asian Summer Monsoon (Wang et al. 2001; Dykoski et al. 2005). In the case of eastern Asia, transmission is through the Northern Hemisphere westerly wind circulation, but this westerly circulation is pinned north of the Himalayas in the northern hemisphere summer, and consequently the Northern Hemisphere westerlies cannot affect the Indian Ocean in this season. Our chironomid record is specifically a summer record. After the resumption of AMOC, summer temperatures at Tiancai Lake started to increase, peaking immediately prior c.16 ka. This coincides with increased SSTs in the Andaman and Arabian Seas (Fig. 4H) and a slow but steady increase in temperature as predicted by the modelling output (Fig. 4E). The large summer temperature variation during H1 at the SE QTP is likely related to the oscillations from the Indian Ocean and the instability of the Indian Ocean (Andaman Sea) Summer Monsoon, exhibiting an interplay of the tropical and high altitude influence of the regional summer temperatures at the site (Fig. 4F and 4H).

449

450 It is widely recognized that North Atlantic Deep Water (NADW) ventilates the circumpolar
451 waters in the Southern Ocean (Howe et al. 2016). About 40% (¬9 Sv) of NADW is believed
452 to upwell south of the polar front in the Southern Ocean today (Iudicone et al. 2008) adding
453 considerable heat to surface waters at high latitudes and thereby plays a role in limiting the
454 extent of winter sea-ice (Weber et al. 2014). A shutdown or reduction of NADW production
455 due to a decline in AMOC before and during HS1 would permit sea-ice to extend further
456 north into the Southern Ocean (e.g. Weber et al. 2014). This would strengthen the
457 circumpolar vortex during the winter, which based on modern observations of the Southern
458 Annular Mode (Stammerjohn et al. 2008) would in turn result in a tightening of the pressure
459 gradient around Antarctica and counterintuitively produce a reduction in the northward
460 penetration of the Southern Hemisphere Winter Westerlies (Montade et al. 2015). A shift of
461 the ITCZ toward the winter (southern) hemisphere would therefore be expected during these
462 periods (centered at around 18, 17 and 15 ka) (De Deckker et al. 2012; Weber et al. 2014),
463 leading to a reduction of the summer monsoonal flow in the Indian Ocean, including the
464 Andaman Sea and summer temperature cooling at Tiancai Lake. While in the Indo-Australian
465 sector, NH impacts on the tropical monsoon can be transmitted directly by the expansion of
466 the Siberian High pressure southwards through the East Asian Winter Monsoon. This is not
467 possible in the Andaman Sea sector because the blocking effects of the QTP and the broader
468 Himalayas limits the southward penetration of the NH westerlies.
469

470 After AMOC resumed during the BA warm period (McManus et al., 2004), the ITCZ shifted
471 northwards, SW China was dominated by the Indian Ocean (Andaman Sea) Summer
472 Monsoon, and the summer air temperature increased to Holocene values in association with
473 an increase in summer monsoon precipitation (Wang et al. 2001) (Fig 1). During the YD cold

event, the $^{231}Pa/^{230}Th$ record from the North Atlantic (Fig. 4F) suggests only a partial reduction of AMOC, in contrast to near complete shut-down during the H1 event (McManus et al. 2004). Consequently, the minor decrease in the summer air temperature around Tiancai Lake indicates that this region was still dominated by a weakened Asian summer monsoon, an observation supported by the pollen record from Nam Co in the southern QTP (Zhu et al. 2015).

In summary, we propose that deglacial summer temperature variability at Taincai Lake is linked to NADW ventilating the Southern Ocean. This causes meridional shifts in the ITCZ in the Indian Ocean sector as the southern hemisphere westerlies contract or expand in response to changes in sea-ice. Though this proposed mechanism is new for the Indian Ocean monsoon(s), a southern hemisphere westerly control of the Australian Summer Monsoon at the LGM has been argued for by Wyrwoll et al. (2012).

5. Conclusions

The chironomid based summer temperature record presented here improves our understanding of subtropical, high-elevation climate change since the LGM on the QTP. This record indicates that summer air temperature was c. 5 °C colder during the LGM, and that it increased rapidly at about 19.0 ka. LGM cooling is attributed in substantial part to a drier regional atmosphere. The switch at 19.0 ka cannot be associated with changes in the northern hemisphere westerlies as chironomids are purely summer proxy. During the last deglaciation, our data detect three millennial scale events including the H1, BA and YD, which align with records from the North Atlantic Ocean and the Indian Ocean (e.g. Tierney et al., 2016), indicating an interaction between the SE Asian tropical climate system and high latitude

499 climate through changing ocean and atmospheric circulation. We propose a ‘new’ mechanism
500 here suggesting that these patterns are linked to North Atlantic Deep water ventilating the
501 Southern Ocean, causing the meridional shift of the ITCZ in the Indian Ocean Basin. Though
502 new for this sector of the Indian Ocean Monsoon, a similar argument has been made for the
503 Australian Summer Monsoon (Wrywoll et al. 2012).
504
505 **Acknowledgments**
506 We thank X.Y. Xiao, Y.L. Li, X. Chen, E.F. Liu, J.J. Wang, and Y. Wang for field assistance
507 and R. Chen for the assistance with drafting Figure 1. This research was supported by the
508 Program of Global Change and Mitigation (2016YFA0600502), the National Natural Science
509 Foundation of China (No. 41272380, 41572337).
510
511 **References**

512 Ahn, J., Wahlen, M., Deck, B.L., Brook, E.J., Mayewski, P.A., Taylor, K.C., White, J.W.C.,
513 2004. A record of atmospheric CO2 during the last 40,000 years from the Siple Dome,
514 Antarctica ice core. Journal of Geophysical Research: Atmospheres 109, D13005.
515 Alley, R. B. 2000. The Younger Dryas cold interval as viewed from central Greenland.
516 Quaternary Science Reviews 19, 213-226.
517 Anderson, J.A., 1984 Regression and ordered categorical variables. Journal of the Royal
518 Statistical Society B46, 1-30.arrows, T. T., G. S. Hope, M. L. Prentice, L. K. Fifield, and S. G.
519 Tims. 2011. Late Pleistocene glaciation of the Mt Giluwe volcano, Papua New Guinea.
520 Quaternary Science Reviews 30, 2676-2689.
521 Berger, A., and M. F. Loutre. 1991. Insolation values for the climate of the last 10 million
522 years. Quaternary Science Reviews 10, 297-317.
523 Birks, H.J.B., 1995. Quantitative paleoenvironmental reconstructions. In: Maddy, D., Brew,
524 J.S., (Eds.)., Statistical Modelling of Quaternary Science Data. Technical Guide 5.
525 Quaternary Research Association, Cambridge, 271pp.
526 Blard, P. H., J. Lave, R. Pik, P. Wagnon, and D. Bourles. 2007. Persistence of full glacial
527 conditions in the central Pacific until 15,000 years ago. Nature 449, 591-594.
528 Bond, G. and others 1997. A Pervasive Millennial-Scale Cycle in North Atlantic Holocene
529 and Glacial Climates. Science 278, 1257-1266.
530 Brooks, S.J., and Birks, H.J.B., 2001. Chironomid inferred air temperatures from Lateglacial
531 and Holocene sites in north-west Europe: progress and problems. Quaternary Science
532 Reviews 20, 1723-1741.
533 Brooks, S.J. and Langdon, P.G. 2014. Summer temperature gradients in northwest Europe
534 during the Lateglacial to early Holocene transition (15-8ka BP) inferred from chironomid
535 assemblages. Quaternary International 341, 80-90.

Brooks, S.J., Langdon, P.G. and Heiri, O., 2007. The identification and use of Palaearctic Chironomidae Larvae in Palaeoecology. Quaternary Research Association, London, UK.
Carlson, A. E., D. W. Oppo, R. E. Came, A. N. LeGrande, L. D. Keigwin, and W. B. Curry. 2008. Subtropical Atlantic salinity variability and Atlantic meridional circulation during the last deglaciation. Geology 36, 991-994.
Chang, J.C., Shulmeister, J. and Woodward, C. 2015. A chironomid based transfer function for reconstructing summer temperatures in south eastern Australia. Palaeogeography, Palaeoclimatology, Palaeoecology, 423, 109-121.
Chen, X., Li, Y., Metcalfe, S., Xaio, X., Yang, X., Zhang, E., 2014a. Diatom response to Asian Monsoon variability during the Late Glacial to Holocene in a small treeline lake, SW China. The Holocene 24, 1369-1377.
Chen, X. M., Chen, F., Zhou, A., Huang, X., Tang, L., Wu, D., Zhang, X., Yu, J., 2014b. Vegetation history, climatic changes and Indian summer monsoon evolution during the Last Glaciation (36,400–13,400 cal yr BP) documented by sediments from Xingyun Lake, Yunnan, China. Palaeogeography, Palaeoclimatology, Palaeoecology 410: 179-189.
Clark, P. U., Shakun, J.D., Baker, P.A., Bartlein, P.J., Brewer, S., Brook, E., Carlson, A.E., Cheng, H., Kaufman, D.S., Liu, Z., Marchitto, T.M., Mix, A.C., Morill, C., Otto-Bleisner, B.L. Pahnke, K., Russell, J.M., Whitlock, C., Adkins, J.F., Blois, J.L., Clark, J., Colman, S.M., Curry, W.B., Flower, B.P.., He, F.,Johnson, T.C., Lynch-Steiglitz, J., Markgraf, V., McManus, J., Mitrovica, J.X., Moreno, P.I., Williams, J.W., 2012. Global climate evolution during the last deglaciation. Proceedings of the National Academy of Sciences 109: E1134-E1142.
CLIMAP Project Members, 1981. Seasonal Reconstructions of the Earth's Surface at the Last Glacial Maximum. Geological Society of America Map Chart Series MC-36, pp. 1–18.
De Deckker P, Moros M, Perner K, Jansen E., 2012. Influence of the tropics and southern westerlies on glacial interhemispheric asymmetry. Nature Geoscience 5,266.
Dutt, S., Gupta, A.K., Clemens, S.C., Cheng, H., Singh, R.K., Kathayat, G., Edwards, R.L., 2015. Abrupt changes in Indian summer monsoon strength during 33,800 to 5500 years B.P. Geophysical Research Letters 42, 5526-5532.
Dykoski, C. A., Edwards, R.L., Cheng, H., Yuan, D., Cai, T., Zhang, M., Lin, Y., Qing, J., An, Z. 2005. A high-resolution, absolute-dated Holocene and deglacial Asian monsoon record from Dongge Cave, China. Earth and Planetary Science Letters 233, 71-86.
Eagle, R. A., Risi, C., Mitchell, J/L., Eiler, J.M., Seibt, U., Neelin, J.D., Li, G., Tripati, A.K., 2013. High regional climate sensitivity over continental China constrained by glacial-recent changes in temperature and the hydrological cycle. Proceedings of the National Academy of Sciences 110, 8813-8818.
Grimm, E.C., 1987. CONISS: a FORTRAN 77 program for stratigraphically constrained cluster analysis by the method of incremental sum of squares. Computers and Geosciences 13, 13-35.
Günther, F., Witt, R., Schouten, S., Mäusbacher, R., Daut, G., Zhu, L., Xu, B., Yao, T., Gleixner, G., 2015. Quaternary ecological responses and impacts of the Indian Ocean Summer Monsoon at Nam Co, Southern Tibetan Plateau. Quaternary Science Reviews 112, 66-77.
Howe, J. N. W., Piotrowski, A.M., Noble, T.L., Mulitza, S., Chiessi, C.M., Bayon, G., 2016. North Atlantic Deep Water Production during the Last Glacial Maximum. Nature Communications 7, 11765.Huguet, C., J.-H. Kim, J. S. Sinninghe Damsté, and S. Schouten. 2006. Reconstruction of sea surface temperature variations in the Arabian Sea over the last 23 kyr using organic proxies (TEX86 and U37K′). Paleoceanography 21, PA3003.
Iudicone, D., Speich, S., Madec, G., Blanke, B., 2008. The Global Conveyor Belt from a Southern Ocean Perspective. Journal of Physical Oceanography 38, 1401-1425.

Kramer, A., U. Herzschuh, S. Mischke, Zhang, G., 2010. Late glacial vegetation and climate oscillations on the southeastern Tibetan Plateau inferred from the Lake Naleng pollen profile. Quaternary Research 73, 324-335.
Kudrass, H.R., Hofmann, A., Doose, H., Emeis, K., Erlenkeuser, H., 2001. Modulation and amplification of climatic changes in the Northern Hemisphere by the Indian summer monsoon during the past 80 ka. Geology 29, 63–66.
Lea, D. W., Pak, D.K., Peterson, I.C., Hughen, K.A., 2003. Synchroneity of Tropical and High-Latitude Atlantic Temperatures over the Last Glacial Termination. Science 301, 1361-1364.
Liu, Z., Otto-Bleisner, B.L, He, F., Brady, E.C., Tomas, R., Clark, P.U., Carlson, A.E., Lynch-Sieglitz, J., Curry, W., Brook, E., Erickson, D., Jacob, R., Kutzbach, J., Cheng, J., 2009. Transient Simulation of Last Deglaciation with a New Mechanism for Bølling-Allerød Warming. Science 325, 310-314.
Liu, Z., S.-I. Shin, B. Otto-Bliesner, J. E. Kutzbach, E. C. Brady, and D. Lee. 2002. Tropical cooling at the last glacial maximum and extratropical ocean ventilation1. Geophysical Research Letters 29:,48-41-48-44.
Loomis, S. E., Russell, J.M., Verschuren, D., Morrill, C., De Cort, G., Sinninghe Damsté, J.S., Olago, D., Eggermont, H., Street-Perrott, F.A., Kelly, M.A., 2017. The tropical lapse rate steepened during the Last Glacial Maximum. Science Advances 3.
MARGO Project Members 2009. Constraints on the magnitude and patterns of ocean cooling at the Last Glacial Maximum. Nature Geosci. 2, 127-132. Mathien-Blard, E. and Bassinot, F. 2009. Salinity bias on the foraminifera Mg/Ca thermometry: Correction procedure and implications for past ocean hydrographic reconstructions. Geochem. Geophys. Geosyst. 10, Q12011
McManus, J. F., R. Francois, J. M. Gherardi, L. D. Keigwin, Brown-Leger, S., 2004. Collapse and rapid resumption of Atlantic meridional circulation linked to deglacial climate changes. Nature 428, 834-837.
Montade, V., Kageyama, M., Cambourie-Nebout, N., Ledru, M-P., Michel, E., Siani, G., Kissel, C., 2015. Teleconnection between the Intertropical Convergence Zone and southern westerly winds throughout the last deglaciation. Geology 43, 735-738.
Oliver, D.R., 1981. Chironomidae. Chapter 29 in : McAlpine, J.F., Peterson, B.V., Shewell, G.E., Teskey, H.J., Vockeroth, J.R., Wood, D.M. (Eds.), Manual of Nearctic Diptera. Agriculture Canada Monograph, Ottawa, Canada. pp 423-458.
Opitz, S., C. Zhang, U. Herzschuh, and S. Mischke. 2015. Climate variability on the south-eastern Tibetan Plateau since the Lateglacial based on a multiproxy approach from Lake Naleng – comparing pollen and non-pollen signals. Quaternary Science Reviews 115, 112-122.
Partin, J. W., Quinn, T.M., Shen, C.C., Okamura, Y., Cardenas, M.B., Siringan, F.P., Banner, J.L., Lin, K., Hu, H.M., Taylor, F.W., 2015. Gradual onset and recovery of the Younger Dryas abrupt climate event in the tropics. Nature Communications 6, 8061.
Pinot, S., Ramstein, G., Harrison, S.P., Prentice, I.C., Guiot, J., Stute, M., Joussame, S., 1999. Tropical paleoclimates at the Last Glacial Maximum: comparison of Paleoclimate Modeling Intercomparison Project (PMIP) simulations and paleodata. Climate Dynamics 15, 857-874.
Porter, S., and An, Z.S.,. 1995. Correlation between climate events in the North Atlantic and China during the last glaciation. Nature 375, 305-308.
Rashid, H., Flower, B.P., Poore, R.Z., and Quinn, T.M., 2007. A ~25 ka Indian Ocean monsoon variability record from the Andaman Sea. Quaternary Science Reviews 26, 2586-2597.

Rievadevall, M., Brooks, S.J., 2001. An identification guide to subfossil Tanypodinae larvae (insecta: Diptera: Chironomidae) based on cephalic setation. Journal of Paleolimnology 25, 81-99.
Rühlemann, C., S. Mulitza, P. J. Müller, G. Wefer, and R. Zahn. 1999. Warming of the tropical Atlantic Ocean and slowdown of thermohaline circulation during the last deglaciation. Nature, 402, 511-514.
Shakun, J. D., Burns, S.J., Fleitmann, D., Kramers, J., Matter, A., Al-Subary, A., 2007. A high-resolution, absolute-dated deglacial speleothem record of Indian Ocean climate from Socotra Island, Yemen. Earth and Planetary Science Letters 259, 442-456.
Shakun, J. D., and Carlson, A.E.. 2010. A global perspective on Last Glacial Maximum to Holocene climate change. Quaternary Science Reviews 29, 1801-1816.
Shakun, J. D., Clark, P.U., He, F., Marcott, S.A., Mix, A.C., Liu, Z., Otto-Bleisner, B., SChmittner, A., Bard, E.,2012. Global warming preceded by increasing carbon dioxide concentrations during the last deglaciation. Nature 484, 49-54.
Shen, C., Liu, K.-b., Tang, L., and Overpeck. J.T., 2006. Quantitative relationships between modern pollen rain and climate in the Tibetan Plateau. Review of Palaeobotany and Palynology 140, 61-77.
Stammerjohn, S. E., Martinson, D.G., Smith, R.C., Yuan, X., Rind, D.,. 2008. Trends in Antarctic annual sea ice retreat and advance and their relation to El Niño–Southern Oscillation and Southern Annular Mode variability. Journal of Geophysical Research: Oceans 113, C03S90.
Tang, H.Q. 2006. Biosystematic study on the chironomid larvae in China (Diptera: Chironomidae). PhD Nankai University, Tianjin, China.
Tierney, J.E. Pausata, F.S.R. and de Menocal, P. 2016. Deglacial Indian monsoon failure and North Atlantic stadials linked by Indian Ocean surface. Nature Geosciences 9, | DOI: 10.1038/NGEO2603.
Tripati, A.K., Sahany, S., Pittman, D. Eagle, R.A., Neelin, D.J., Mitchell, J.L. and Beaufort, L. 2014. Modern and glacial tropical snowlines controlled by sea surface temperature and atmospheric mixing. Nature Geosciences 7, 205–209.
Wang, T., Liu, Y., Huang, W., 2013. Last Glacial Maximum Sea Surface Temperatures: A Model-Data Comparison, Atmospheric and Oceanic Science Letters, 6, 233-239.
Wang, Y., Herschuh, U., Shumilovskikh, L.S., Mischke, S., Birks, H.J.B., Wischnewski, J., Bδhner, J., Schùtz, F., Lemkuhl, F., Diekmann, B., Wùnnermann, B., Zhang, C., 2014. Quantitative reconstruction of precipitation changes on the NE Tibetan Plateau since the Last Glacial Maximum; extending the concept of pollen source area to pollen-based climate reconstructions from large lakes. Climate of the Past 10, 21-39.
Wang, Y.J., Cheng, H., Edwards, R.L., An, Z.S., Wu, J.Y., Shen, C.C., Dorale, J.A., 2001. A High-Resolution Absolute-Dated Late Pleistocene Monsoon Record from Hulu Cave, China. Science 294:,2345-2348.
Weber, M.E., Clark, P.U., Kuhn, G., Timmermann, A., Sprenk, D., Gladstone, R., Zhang, X., Lohmann, G., Menvial, L., Chikamoto, M.O., Friedrich, T., Ohlwein, C., 2014. Millennial-scale variability in Antarctic ice-sheet discharge during the last deglaciation. Nature 510: 134-138.
Wyrwoll, K.-H., Hopwood, J.M. and Chen, G. 2012: Orbital time-scale circulation controls of the Australian summer monsoon: a possible role for mid-latitude Southern Hemisphere forcing? Quaternary Science Reviews 35, 23-28.
Xiao, X., Haberle, S.G., Shen, J., Yang, X., Han, Y., Zhang, E., Wang, S., 2014a. Latest Pleistocene and Holocene vegetation and climate history inferred from an alpine lacustrine

683 record, northwestern Yunnan Province, southwestern China. Quaternary Science Reviews 86,
684 35-48.
685 Xaio, X., Haberle, S.G., Yang, X., Shen, J., Han, Y., Wang, S., 2014b. New evidence on
686 deglacial climatic variability from an alpine lacustrine record in northwestern Yunnan
687 Province, southwestern China. Palaeogeography, Palaeoclimatology, Palaeoecology 406, 9-
688 21.
689 Yancheva, G., Nowaczyk, N.R., Mingram, J., Dulski, P., Schettler, G., Negendank, J.F.W.,
690 Liu, J., Sigman, D.M., Peterson, L.C., Haug, G.H., 2007. Influence of the intertropical
691 convergence zone on the East Asian monsoon. Nature 445, 74-77.
692 Zhang, E., Chang, J., Cao, Y., Sun, W., Shulmeister, J., Tang, H., Langdon, P.G., Yang, X.,
693 Shen, J., 2017a. A chironomid-based mean July temperature inference model from the south-
694 east margin of the Tibetan Plateau, China. Climate of the Past 13, 185-199.
695 Zhang, E., Chang, J., Cao, Y., Tang, H., Langdon, P.J., Shulmeister, J., Wang, R., Yang, X.,
696 Shen, J., 2017b. Holocene high-resolution quantitative summer temperature reconstruction
697 based on subfossil chironomids from the southeast margin of the Qinghai-Tibetan Plateau.
698 Quaternary Science Reviews 165, 1-12.
699 Zhang, R., and T. L. Delworth. 2005. Simulated Tropical Response to a Substantial
700 Weakening of the Atlantic Thermohaline Circulation. Journal of Climate 18, 1853-1860.
701 Zhang, W., Cui., Z., Feng, J., Yi., C., Yang, J. 2005. Late Pleistocene glaciation of the
702 Hulifang Massif of Gongwang Mountains in Yunnan Province, Journal of Geographical
703 Sciences 15, 448-458.
704 Zhu, L., Lu, X., Wang, J., Peng, P., Kasper, T., Daut, G., Haberzettl, T., Frenzel, P., Li, Q.,
705 Yang, R., Schwalb, A., Mäusbacher, R. 2015. Climate change on the Tibetan Plateau in
706 response to shifting atmospheric circulation since the LGM. Scientific reports 5, 13318.
707

708 **Figure Captions**

709

710 Fig. 1. Map showing the locations of Tiancai Lake (red square) and other palaeoclimate study
711 sites referenced in the text. Locations of marine core OCE326-GGC5 (McManus et al. 2004),
712 Greenland ice core North Greenland Ice Core Project (NGRIP) (Alley, 2000), Hulu cave
713 (Wang et al. 2001), Dongge cave (Dykoski et al. 2005), Mawmluh cave (Dutt et al. 2015),
714 marine core P178-15P (Tierney et al., 2016), marine core RC12-344 (Rashid et al. 2007), and
715 Antarctic ice core Siple Dome (Ahn et al. 2004) are marked in closed circles. We have
716 overlaid the map with a cartoon of our proposed link between NADW and the Indian
717 monsoon in the Andaman Sea. This cartoon highlights the effect of changing Atlantic
718 Meridional Circulation (AMOC) on the Indian Ocean Monsoon. (A) at times of strong
719 AMOC, upwelling in the Southern Ocean limits sea-ice extent. This results in a broad zone of

720 Southern Hemisphere westerly activity that extends further into the sub-tropics and helps
721 keep the ITCZ north during the SH winter. This enhances the summer monsoon (SW) in the
722 Indian Ocean. At times of weakened AMOC, less upwelling occurs in the Southern Ocean
723 and sea-ice expands. Counterintuitively, though this strengthens westerly circulation it also
724 tightens the zone of westerly flow (e.g. Stammerjohn et al., 2008) allowing the ITCZ to move
725 further south, thereby weakening the Indian Ocean Monsoon.
726

727 Fig. 2. A percentage summary diagram of chironomid head capsules taxa recovered from the
728 Tiancai Lake core material covering the period between 19.5 and 8 ka. 30 major (occurrences
729 higher than 10% in at least 10 samples) taxa were displayed (the full diagram is referred to
730 Figure S1). The record was divided into five distinct zones using a stratigraphic cluster
731 analysis based on the change of the chironomid asemblages. The diagram displays a rapid
732 transition from cold conditions at the base of the record, The Holocene part of this record is
733 published in Zhang et al. (2017b). The full details on the radiocarbon chronology are
734 published in Xiao et al. (2014b).
735

736 Fig. 3. Reconstruction diagnostics for Tiancai Lake fossil samples between 19.5 and 8 ka.
737 (**A**). Goodness-of-fit statistics where the fossil samples are passively fitted to the constrained
738 ordination axis derived from the modern training set to mean July temperatures (MJTs). The
739 vertical dashed line represents the 95^{th} percentiles of modern squared residual lengths beyond
740 which fossil samples are considered to have 'poor fits' to MJTs. (**B**). Trajectory changes of
741 trend through time of fossil samples covering 19.5-8 ka (blue line) in the Tiancai Lake
742 record, passively plotted in a redundancy analysis of the 100 training set lakes (open green
743 circles), where changes in trend tracks the MJT gradient between 7-11 °C (red lines),
744 indicating that MJT is a primary controlling variable and drives the changes of chironomid

745 assemblages of these fossil samples. (**C**). The assessment of the quality of analogues where
746 squared residual length of Tiancai Lake fossil samples were plotted against chronology.
747 Fossil samples with 'good' modern analogues are shown in the blue shaded area, whereas
748 fossil samples with 'fair' and 'none' modern analogues are displayed in the yellow and red
749 areas respectively. The blue, yellow and red shaded areas represent the 5^{nd}, 15^{th} percentiles
750 and beyond respectively.
751
752 Fig. 4. **(A).** Tiancai Lake chironomid-mean July temperature record covering 19-8 ka (red
753 line; this study) and part of the Holocene (grey line; Zhang et al. 2017a). These are compared
754 against other proxy and model records from the same site, surrounding regions and the globe:
755 **(B)**. Pollen accumulation rate at Tiancai Lake (Xiao et al. 2014); **(C).** The NGRIP $\delta^{18}O$
756 record from Greenland (Alley, 2000); **(D)**. Northern Hemisphere (red line) and Atlantic (blue
757 line) temperature anomalies (Shakun et al. 2012); **(E)**. Modelled temperature response
758 included forcings of CO_2, solar insolation, meltwater flux and ice sheets using the
759 Community Climate System Model version 3 (CCSM3) (Liu et al. 2009). The output data
760 were calculated for the latitude of Tiancai Lake, at 26°N; **(F)**. $^{231}Pa/^{230}Th$ record of North
761 Atlantic (McManus et al. 2004), a proxy for AMOC; **(G)**. Sub-tropical Atlantic sea surface
762 temperature (SST) reconstructed based on Mg/Ca ratio (Carlson et al. 2008); **(H)**. SST
763 reconstructed from Arabian Sea (Pink) (Tierney et al., 2016)and Andaman Sea (green)
764 (Rashid et al. 2007). Both reconstructions are based on paired Mg/Ca and $\delta^{18}O$ data of the
765 planktic foraminifer *Globigerinoides ruber*. **(I)**. Summer insolation curve for 30 °N **(J)**.
766 Speleothem $\delta^{18}O$ records from Hulu (pink line) and Dongge (black line) Caves in the eastern
767 and southern China (Dykoski et al. 2005; Wang et al. 2001), and Mawmluh Cave (blue line)
768 from northern India (Dutt et al. 2015); **(K)**. CO_2 concentration from Antarctic ice core record
769 (Ahn et al. 2004). Blue shading is utilised to represent 'cold' events in the North Atlantic.

Figure 1

Click here to download high resolution image

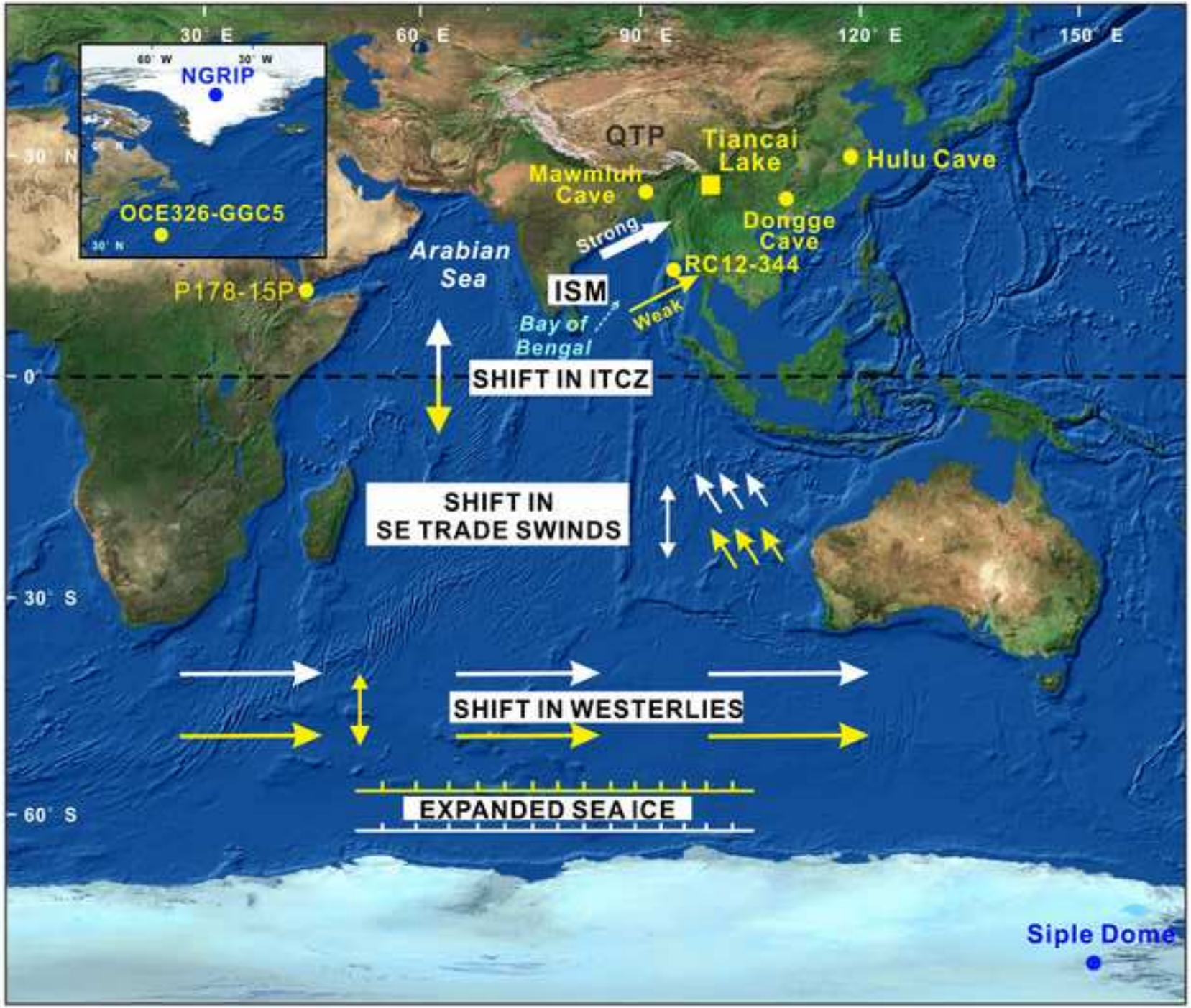

Figure 2

Click here to download high resolution image

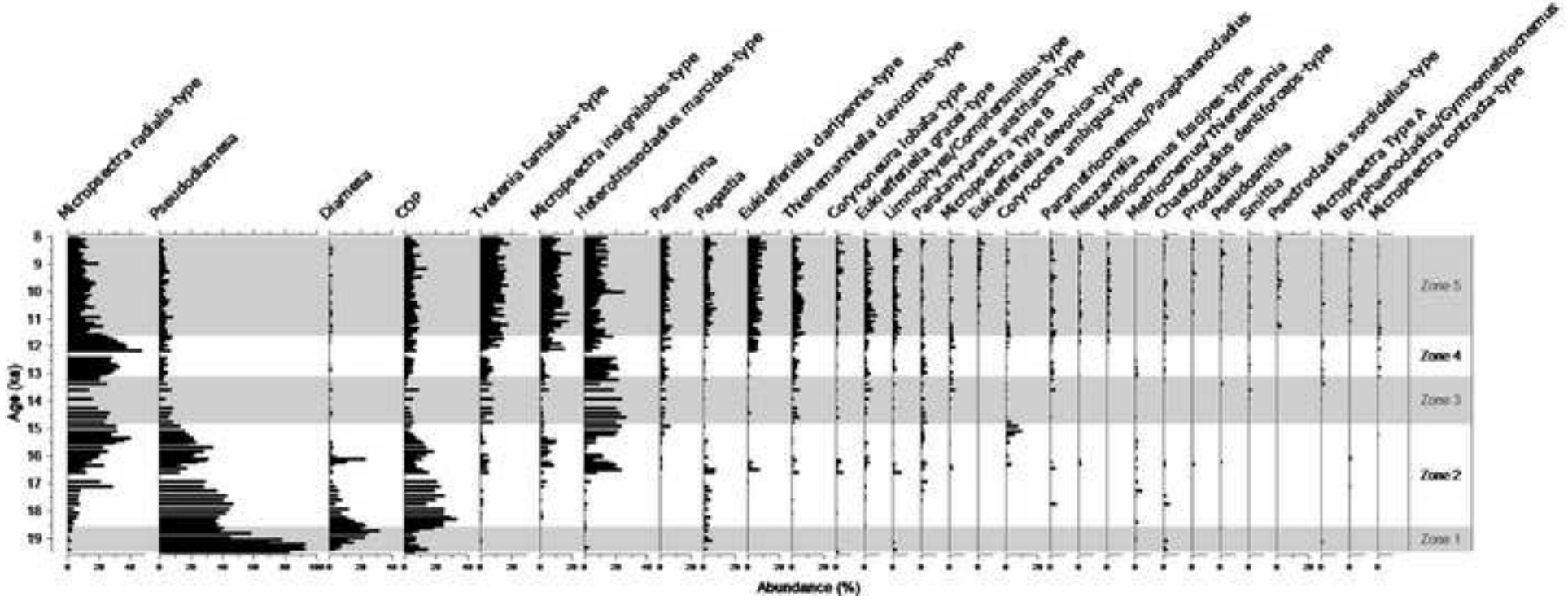

Figure 3

Click here to download high resolution image

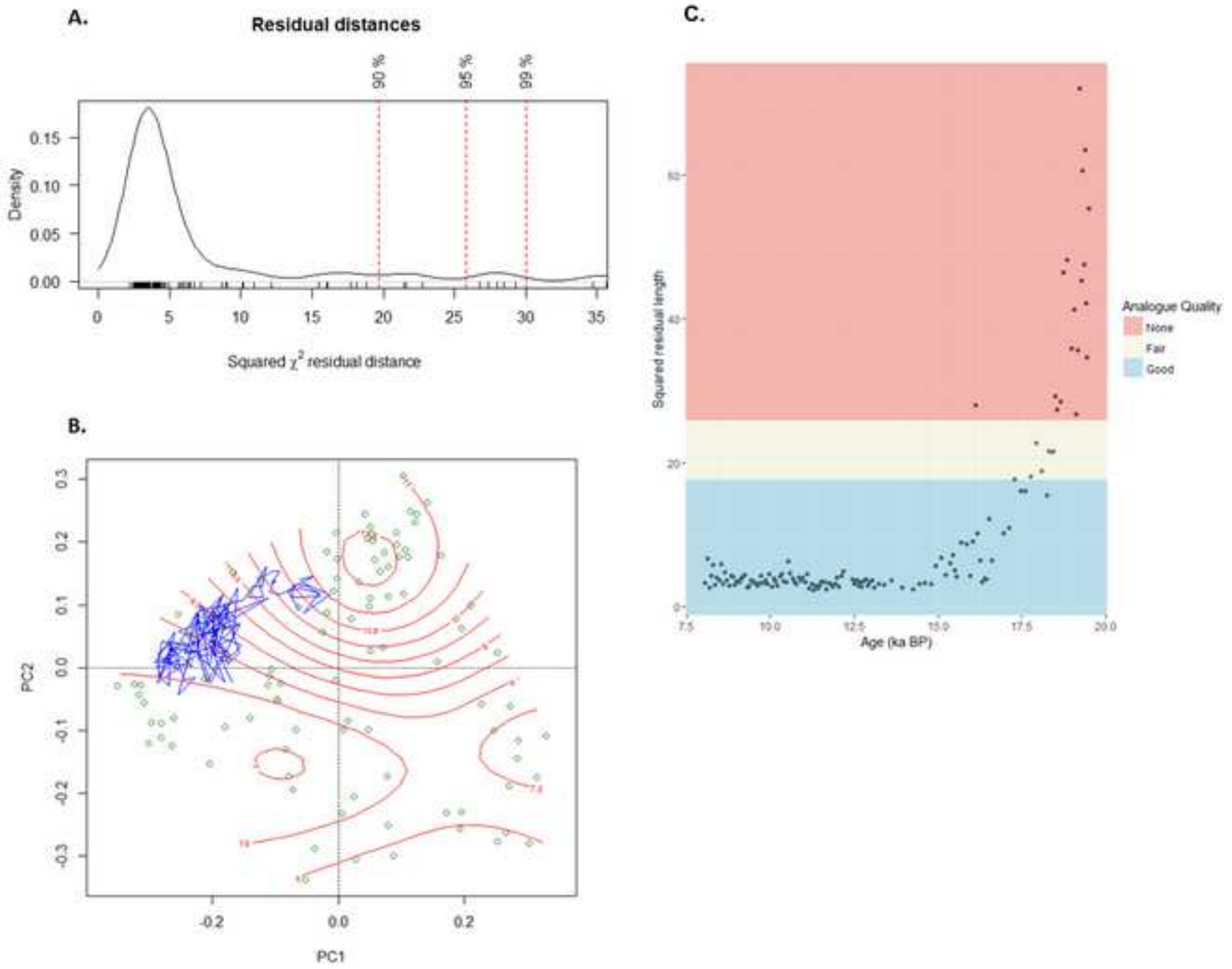

Figure 4

Click here to download high resolution image

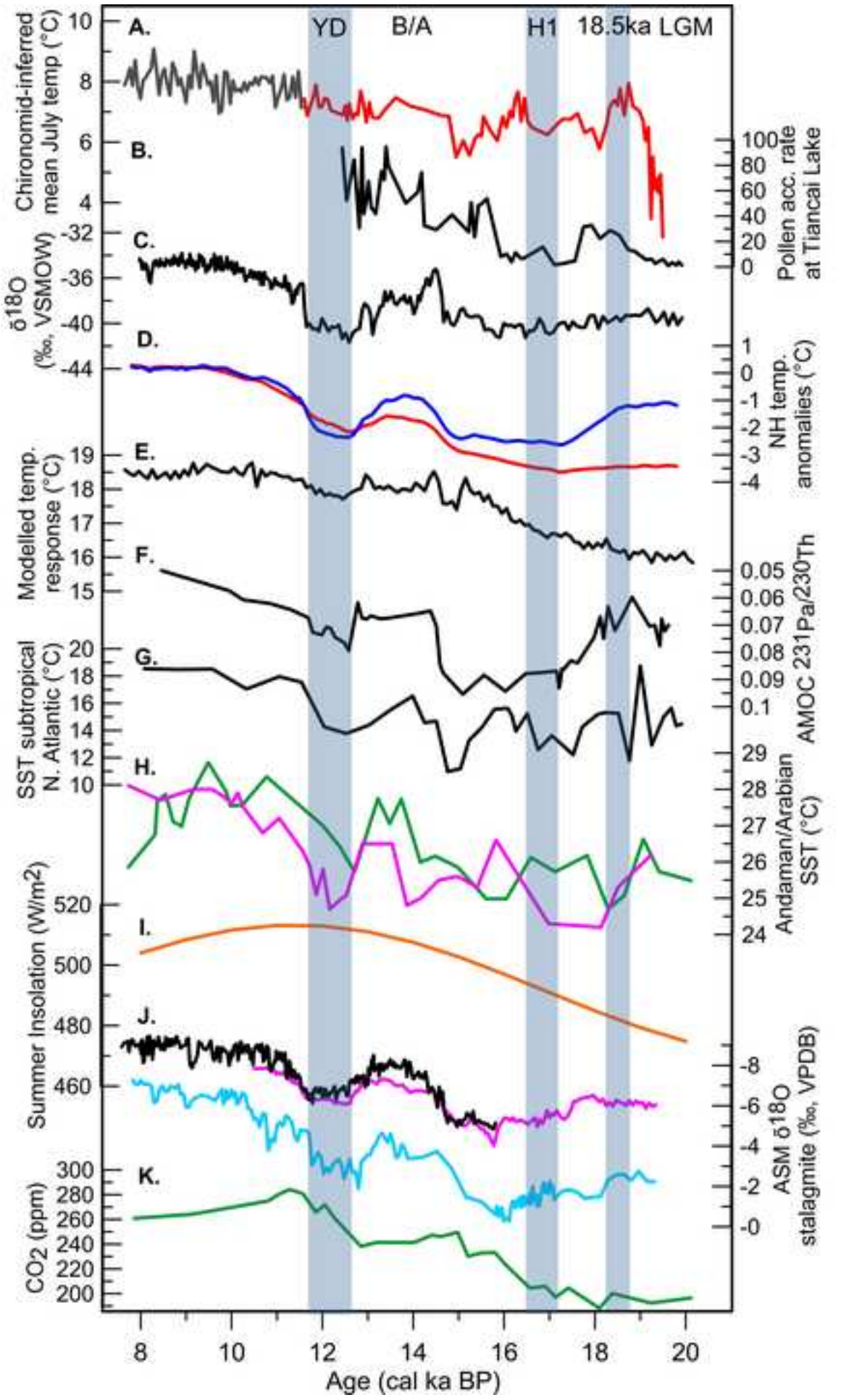

Supplementary Figure 1

Click here to download Supplementary material for online publication only: Supplementary data-EPSL-Zhang et al.docx